Temperature dependence of tropospheric ozone under NO$_x$ reductions over Germany

Noelia Otero [a,b,*], Henning W. Rust [b], Tim Butler [a,b]

[a] Institute for Advanced Sustainability Studies, Potsdam, Germany
[b] Institut Für Meteorologie, Freie Universität Berlin, Germany

HIGHLIGHTS

- The observed climate penalty of ozone has decreased over the past decades in a large number of German stations.
- There is a decreasing temperature dependence of ozone at moderate-high temperatures.
- Emissions reductions have been generally effective in the southwestern regions of Germany.
- In Berlin, additional emission reductions should be required to mitigate the climate penalty of ozone.

ARTICLE INFO

ABSTRACT

Due to the strong temperature dependence of surface ozone concentrations (O$_3$), future warmer conditions may worsen ozone pollution levels despite continued efforts on emission controls of ozone precursors. Using long-term measurements of hourly O$_3$ concentrations co-located with NO$_x$ concentrations in stations distributed throughout Germany, we assess changes in the climate penalty in summertime, defined as the slope of ozone-temperature relationship during the period 1999–2018. We find a stronger temperature sensitivity in the urban stations over the southwestern regions, especially in the first period of the study (1999–2008). We show a decrease in the climate penalty in most of stations during the second period of the study (2009–2018), with some exceptions (e.g. Berlin) where the climate penalty did not show significant changes. A key motivation of this study is to provide further insights into the impacts of NO$_x$ reductions in the O$_3$-temperature relationship. For that, we propose a statisti-cal approach based on Generalized Additive Models (GAMs) to describe ozone pro-duction rates, inferred from hourly observations, as a function of NO$_x$ and temperature, among other variables relevant during the O$_3$ production. The GAMs confirm lower O$_3$ production rates during the second period (2009–2018) at most of the stations and a decreasing sensitivity to temperature. We observe that a large number of stations are transitioning to NO$_x$-limited chemistry, consistent with a decreasing temperature dependence of O$_3$ at moderate-high temperatures as a result of sustained NO$_x$ reductions. Moreover, the GAMs results showed changes in the shape of the function representing the O$_3$-temperature relationship when comparing the first and second period, which suggest changes in VOC influencing the temperature dependence of O$_3$. From these results, we infer effective VOC reductions over time that have also contributed to the observed decrease of O$_3$ production rates. Thus, our analysis indicates that emissions reductions have been effective in a number of stations, particularly in the southwestern regions. However, we notice that in a few stations (e.g. Berlin) additional emission reductions should be required to effectively mitigate the temperature dependence of O$_3$.

1. Introduction

Tropospheric ozone (O$_3$) is a secondary pollutant formed from complex photochemical reactions of nitrogen oxides (NO$_x$), carbon monoxide (CO) and volatile organic compounds (VOCs) in the presence of sunlight (Seinfeld & Pan-dis, 2006). Changes in emissions of two of its major precursors, NO$_x$ and VOCs, might alter ozone formation regimes that are controlled by the initial NO$_x$/VOC ratio (Sillman, 1999). Large

---

NO_x emissions and concentrations favour a VOC- sensitive regime, while large VOC emissions and concentrations, and HO_x pro-duction rates favour a NO_x-sensitive regime (Pusede et al., 2015; Sillman, 1999).

The chemistry of O_3 production varies nonlinearly with temperature, which speeds up the rate of many chemical reactions. Furthermore, emissions of O_3 precursors from many anthropogenic and biogenic sources are strongly related to temperature. Pusede et al. (2014) examined changes in organic emissions by using a temperature-response framework and they found that the total organic reactivity experimented larger decreases from 2000 to 2010 at lower temperatures (emissions of temperature independent organic reactivity) than at higher tem-peratures (emissions of temperature dependent organic reactivity). Butler et al. (2020) showed that the local photochemical production of maximum ozone in the Northern Hemisphere in summertime is mainly due to the combination of lo-cal emissions of anthropogenic NO_x and biogenic VOC. Moreover, they pointed the significant role played by biogenic VOC in summer. Due to the strong dependence of biogenic VOC emissions on temperature and solar radiation, bio-genic VOC, such as isoprene, are expected to be relevant for O_3 production, particularly in summer days (Guenther et al., 2006). Therefore, O_3 production is highly sensitive to meteorological parameters, specifically temperature, and thus, changes in ambient conditions and precursor emissions are nonlinear and complex.

A wide number of studies have shown that the O_3-temperature relationship varies in space and time due to differing chemical and meteorological mech-anisms that influence O_3 formation (Bloomer et al., 2010; Rasmussen et al., 2013; Steiner et al., 2010). It has been recognized the temperature dependence of biogenic VOC emissions as well as the sensitivity of O_3 production to temperature to the peroxy acyl nitrate (PAN) dissociation rates (Jacob et al., 1993; Jacob and Winner, 2009; Sillman and Samsom, 1995). Moreover, dry deposition (Wesely, 1989) and NO_x emissions (Coates et al., 2016) can contribute to the O_3-temperature relationship. Pusede et al. (2015) provides a comprehensive re-view of the temperature dependence of O_3 production. They pointed out that changes in O_3 precursors under a warmer climate will affect O_3 production in a predictable but complex way. For example, the continued NO_x reductions in urban areas would lead to a transition in the chemistry of O_3 production into chemical regimes typically observed in rural areas.

Romer et al. (2018) investigated the effect of temperature in O_3 produc-tion using measurements in a rural site over the southeastern United States. They found that local chemistry were key drivers of increased O_3 concentrations on hotter days, and a large proportion of this increase was attributable to temperature-driven increases in soil emissions of NO_x. Recent modelling studies have examined the processes driving the O_3-temperature relationship. Porter and Heald (2019) used model simulations to quantify the contribution of mechanisms driving the O_3-temperature relationship. They found that a large proportion of the O_3-temperature relationship might be explained by other meteorological phenomena such as stagnation and humidity over Europe. Stagnant conditions characterised by low wind speed, allow O_3 to build up to high levels. Similarly, Leibensperger et al. (2008) showed that the frequency of summertime cyclones is a good predictor of stagnant conditions and high O_3 pollution in the eastern United States. High levels of humidity have certain scavenging effect on O_3, as higher humidity is usually associated to greater cloud cover and atmospheric instability that can inhibit photochemical reactions and hence, decrease O_3. Kerr et al. (2019) performed sensitivity simulations to examine the role of the processes related to the O_3-temperature relationship over the United States, focusing on transport, chemistry and anthropogenic emissions. They found that atmospheric transport played a significant role in explaining the O_3-temperature relationship through out much of the United States. Since transport is indirectly related to temperature, the authors highlighted the importance of providing a better understanding of the changes in the mechanisms linking transport and O_3 in a warmer climate.

Under future climate conditions, the benefits from control strategies of ozone precursors might be countered by temperature increases (Rasmussen et al., 2013). This effect has been termed in the literature as a "climate penalty", which has been used to quantify the additional increase of O_3 or the reduced benefits of emissions controls as a result of climate change (Rasmussen et al., 2013; Wu et al., 2008). While most of the observational and modelling studies Bloomer et al. (2009); Rasmussen et al. (2013); Steiner et al. (2010) have reported a decreasing sensitivity of O_3 to temperature due to the emission reductions, there are some exceptions that pointed out that the climate penalty could be aggravated by weather conditions (Jing et al., 2017; Boleti et al., 2020). Previous studies have shown that feedbacks from vegetation worsen peak O_3 episodes especially during extreme hot and dry periods over Europe (Gerosa et al., 2009; Lin et al., 2020). Moreover, soil moisture deficit is a relevant factor of stress for isoprene emissions (Guenther et al., 2006). Severe droughts might influence plant growth and limit biomass production, which can lead to a reduction of isoprene emission (Emmerson et al., 2019). Lin et al. (2020) examined the contribution of drought to the O 3 climate penalty over the past six decades over Europe using numerical simulations. They highlight the importance of considering land-atmospheric interactions and they showed that reduced ozone removal by water-stressed vegetation due to dry conditions, exacerbate ozone air pollution over Europe.

According to the EuroDelta-Trends modelling experiment (ETC/ACM), Colette et al., (2017) the reduction of European anthropogenic emissions of O_3 precursors was the main factor in decreasing summertime O_3 peaks episodes during the period 1990–2010. Previous studies have shown general downward trends of O_3 concentrations for the past decades Chang et al. (2017); Fleming et al. (2018). However, O_3 levels have not decreased as expected (EEA, 2020), in particular in urban areas as a results to lower tritration processes (Querol et al., 2016; Yan et al., 2019). Recent trends analysis indicated a clearer de-creasing trend of O_3 peaks during 2000–2008 over most of the European sites, but not significant trends during 2009–2018 and mostly flattering since 2009 (EEA, 2020). With the current regulation of emission of O_3 precursors, such contrasting trends found across European sites along with the observed changes in the O_3 sensitivity to temperature, provide an ideal scenario for investigating the O_3-temperature relationship.

The primary objective of this study is to assess the observed changes in the O_3 climate penalty and the impacts of NO_x reductions on the temperature dependence of O_3 for the last two decades. We use long-term O_3 concentrations over Germany where the temporal homogeneity and diversity of the data offer an unique opportunity for long-term analysis of O_3 and NO_x. We examine changes in the O_3-temperature relationship over a 20-year time period covered 1999 to 2018, for which a greater number of sites were available. For that, we split the complete period into two periods (1999–2008, 2009–2018), as a 10-year period is long enough to assess changes in O_3 behaviour (Sicard et al., 2009). Furthermore, we restrict our study to summertime when O_3 normally reaches the highest levels and the photochemical activity is higher (Pusede et al., 2015). In addition, it has been shown a stronger temperature dependence of O_3 over Ger-many in summertime (Otero et al., 2018). We begin our study by calculating the trends in NO_x concentrations that might lead to changes in the O_3-temperature relationship. Since the variability of O_3 production can explain a considerable proportion of O_3-temperature relationship (Pusede et al., 2015), we propose an observational-based statistical modelling approach to examine the nonlinear dependence of O_3 production on NO_x-temperature relationship. Within a sta-tistical modelling framework built upon Generalized Additive Models (GAMs), we infer O_3 production (as a rate of change of O_3, ΔO_3) from hourly O_3 con-centrations. Thus, we model ΔO_3 as a function of temperature and NO_x along with other critical variables during the O_3 formation. Ultimately, we aim to pro-vide new insights into the O_3 response to changes of its precursors in different environments and the effectiveness of emission reductions.

2. Data

Hourly measurements of O_3 and NO_x concentrations were extracted from the European Environment Agency's (EEA) public air quality database "Air- Base" (https://www.eea.europa.eu/data-and-maps/data/aqereporting-8). The number of sites and length of the period covered by each station for which measurements are available vary spatially and greatly by pollutant. The selection of the monitoring stations with co-located data (O_3 and NO_x) was based on the station type (background), station type area (rural, urban, suburban) and altitude (< 1000 m). Only the stations reporting more than 75% of valid data out of all the possible data in each summertime were included in the study. We use the stations with at least 19 years with hourly co-located data within the whole period of study defined from 1999 to 2018. Here, summertime is referred to July-August-September (JAS), with a strong O_3-temperature relationship, particularly in Central Europe (Otero et al., 2018). A total of 29 stations meet the pre-processing criteria: 15 rural, 12 urban and 2 suburban stations. Despite that the spatial distribution of the measurement sites is not uniform with the largest density of stations over west and central Germany, a representative number of stations covering eastern regions are included (Fig. 1). Daily means and daily maximum of the running 8-h mean of O_3 (MDA8) were calculated fol-lowing the European Union Directive of 2008 procedure (European Parliament and Council of the European Union, 2008).

The meteorology was extracted from the ERA5 Herbach and Dee (2016), the latest climate reanalysis produced by the European Centre for Medium Range Weather Forecast (ECMWF) that provides hourly data on regular latitude-longitude $0.25° \times 0.25°$ spatial resolution. The variables included in the analysis are air surface 2 m-temperature (°C), 10 m u and v-component of wind (ms^{-1}), boundary layer height (m) and relative humidity at 1000 hPa (%).
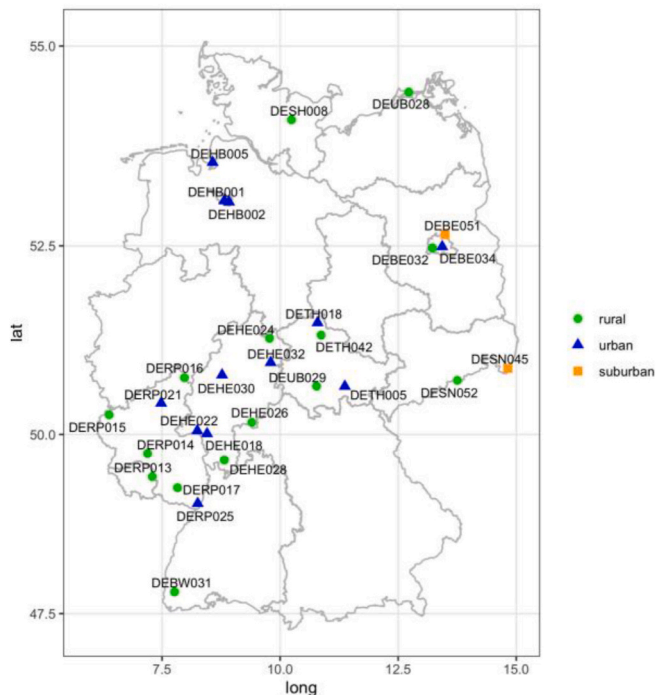
3. Methods

3.1. Climate penalty

A number of definitions have been used in the literature to characterise the ozone climate penalty, usually represented as the linear relationship between O_3 and temperature. Climate penalty values are normally computed using daily maximum summertime O_3 observations (1 or 8 h average) and daily maximum temperature, although there is no standard definition (Pusede et al., 2015).

Here, we adopted one of the most common metric to represent the climate penalty (hereinafter, $m_{O3\ T}$) as the slope of the best fit line between long-term MDA8 concentrations and daily maximum temperature (Bloomer et al., 2009; Otero et al., 2018; Steiner et al., 2010). We first calculated the $m_{O3\ T}$ using Ordinary Least Squares (OLS) regression applied separately for each station and each period (1999–2008, 2009–2018). The general equation for the linear model can be written as follows:

$$MDA8(t) = a + m_{O3\ T}\ T(t) + E(t) \tag{1}$$

With $E(t) \sim N(0, \sigma^2)$ being a sequence of independent Gaussian random variables with zero expectation. MDA8(t), T(t) are the time series of MDA8 and daily maximum temperature (respectively) and a represents the intercept. We estimate the climate penalty separately for the periods 1999–2008 and 2009–2018 and the significant differences between the slopes in both periods are assessed through a *t*-test at the 95% confidence level of statistical significance.

3.2. Approximation of O_3 production rates from observations

Most of the previous works have used numerical models (Steiner

Code	Station name	Station type area	Longitude	Latitude
DEBE032	Berlin-Grunewald	rural	13.23	52.47
DEBE034	Berlin-Neukölln-Nansenstraße	urban	13.43	52.49
DEBE051	Berlin-Buch	suburban	13.49	52.64
DEBW031	Schwarzwald-Süd	rural	7.76	47.81
DEHB001	Bremen-Mitte	urban	8.82	53.08
DEHB002	Bremen-Ost	urban	8.92	53.06
DEHB005	Bremerhaven	urban	8.57	53.56
DEHE018	Raunheim	urban	8.45	50.01
DEHE022	Wiesbaden-Süd	urban	8.24	50.05
DEHE024	Witzenhausen/Wald	rural	9.77	51.29
DEHE026	Spessart	rural	9.40	50.16
DEHE028	Fürth/Odenwald	rural	8.82	49.65
DEHE030	Marburg	urban	8.77	50.80
DEHE032	Bebra	urban	9.80	50.97
DERP013	Westpfalz-Waldmohr	rural	7.29	49.42
DERP014	Hunsrück-Leisel	rural	7.19	49.74
DERP015	Westeifel Wascheid	rural	6.38	50.27
DERP016	Westerwald-Herdorf	rural	7.97	50.77
DERP017	Pfälzerwald-Hortenkopf	rural	7.83	49.27
DERP021	Neuwied-Hafenstraße	urban	7.48	50.42
DERP025	Wörth-Marktplatz	urban	8.25	49.05
DESH008	Bornhöved	rural	10.24	54.09
DESN045	Zittau-Ost	suburban	14.82	50.89
DESN052	Zinnwald	rural	13.75	50.73
DETH005	Saalfeld	urban	11.37	50.65
DETH018	Nordhausen	urban	10.79	51.50
DETH042	Possen	rural	10.87	51.33
DEUB028	Zingst	rural	12.72	54.44
DEUB029	Schmücke	rural	10.77	50.65

Fig. 1. Spatial distribution of the monitoring stations used in the study along with the metadata information: code, station name, type area and coordinates.

et al., 2006), box model (Coates et al., 2016), plume model (LaFranchi et al., 2011) or analytical models (Pusede et al., 2014; Romer et al., 2018) to analyse the temperature-dependent mechanisms affecting the O_3 production. Here, we propose a new approach based on GAMs to examine changes in the O_3 production. We approximate the latter by the rate of change of hourly O_3 concentrations as:

$$\Delta O_3(t) = O_3(t) - O_3(t-1) \qquad (2)$$

The general O_3 budget equation can be expressed as:

$$dO_3/dt = PO_{3chem} + LO_{3chem} + MD \qquad (3)$$

PO_{3chem} represents the chemical O_3 production rate, LO_{3chem} is the chemical loss rate and the last term MD represents the dynamical processes that influence O_3 concentrations, including mixing and dry deposition processes. These individual processes can vary in strength and by location throughout the day.

As we aim to assess how NO_x reductions influence the sensitivity of O_3 to temperature, we restrict our analysis to a time interval with an intense pho-tochemical activity, which usually coincides with higher O_3 concentrations and warmer temperatures. Thus, the data was filtered to avoid including non-related photochemical processes that might mask the photochemistry in the daily O_3 production. First, we selected data after sunrise and until O_3 reaches the daily maximum value (usually in the afternoon). In order to exclude some maximum values that might occur late in the afternoon or evening and are mostly related to prevailing meteorological conditions and transport processes (Kulkarni et al., 2013), the time was restricted to 17:00 H (local time). Then, a wind speed condition was used to exclude the hourly data when wind speed was higher than 3.2 ms^{-1}, which is the threshold value usually applied to define stagnant conditions (Horton et al., 2014). After a first inspection of the data, we found consider-able differences in the minimum of NO_x concentrations across some stations and periods, likely due to the detection methods. To better establish a comparison between stations and periods, we applied an additional filter to remove NO_x values below 5 µgm^{-3}. It must be noted that the NO_x cut-off filter had an impact in a few rural stations, for which the percentage of surviving data to the filter was smaller. However, it does not affect the results and conclusions presented here. The number of observations that met these conditions varies with each station type and on average a 20% (urban), 14% (rural), 18% (suburban) of the total data was used.

3.3. Modelling O_3 production rates with GAMs

GAMs (Hastie and Tibshinari, 1990; Wood, 2006) were used to examine variations in $\Delta O_3(t)$ over the last two decades and the changes in the relationship NO_x-temperature given the observed downward trends of the O_3 sensitivity to temperature in the two periods of study 1999–2008 and 2009–2018. These periods were selected as a compromise between robustness and homogeneity (Solberg et al., 2018). A 10-year period is long enough for modelling purposes and for assessing changes in ozone behaviour (Sicard et al., 2009), and a decade states that the ozone response with respect to the covariates is consistent through the period of study (Solberg et al., 2018). GAMs are useful tools for estimating non-parametric relationships whilst retaining clarity of interpretation (Wood, 2006). The relationship between the explanatory variables (henceforth covariates) and the response is described by smooth curves (splines, or potentially other smoothers). Such models have proven useful for studying the complex non-linear relationships between atmospheric chemical species and meteorological parameters (Barmpadimos et al., 2011; Boleti et al., 2019; Carslaw et al., 2007; Jackson et al., 2009). In the frame of GAMs a model for the expectation μ of a random variable $Y \sim N(\mu, \sigma^2)$ can be written as

$$g(\mu) = \beta_0 + f_1(X_1) + f_2(X_1) + \ldots \qquad (4)$$

Where g is static link function, X_n are the covariates and f_n are the non-

parametric smoothing functions; β_0 is the intercept. If the response can be assumed to be normally distributed, the canonical link function is the identity. After a closer inspection of the residuals at the individual sites, we found non-normally distributed residuals with problems in the tails. Thus we used a scaled t distribution instead, which is recommended for heavy tailed response variables (Wood et al., 2016). To include non-linear interactions between covariates, tensor products were used as smoothers, e.g.,

$$g(\mu) = \beta_0 + f_1(X_1, X_2) + \ldots . \qquad (5)$$

This describes a nonlinear relationship between the response and 2 covariates (interaction) (Wood, 2006). The smoothness of each function is controlled by the number of knots or effective number of degrees of freedom. Here, the smoothing parameters were estimated by restricted maximum likelihood (REML) (Wood, 2006).

The challenge in building a model that captures a large proportion of the variability of ΔO_3 is to select the key covariates out of a large number of poten-tial variables. As stated in the previous section, changes in O_3 concentrations depend on local production, involving many chemical reactions that vary with temperature, loss mechanisms that are sensitive to meteorological conditions and transport processes. Therefore, we chose the variables that are expected to have a major influence on O_3 production (e.g. NO_x). The photochemical nature of O_3 production is strongly influenced by temperature (tas). In partic-ular, emissions of some biogenic VOC, such isoprene, are well known to increase with temperature (Coates et al., 2016; Pusede et al., 2014). Thus, we use temperature as a surrogate to represent changes in VOC, which can be emitted as an exponential function of temperature (LaFranchi et al., 2011; Pusede et al., 2014).

Daytime variation in the boundary layer height (BLH) significantly con-tributes to changes in O_3 production rates that tend to increase with a deepening BLH during sunny and warm days (Haman et al., 2014). In addition to chemical and mixing processes, changes in O_3 concentrations are influenced by deposition. Therefore, additional covariates are the percentage of change of the boundary layer height growth rate (ΔBLH) (in %) accounting for mixing processes, and vapor pressure deficit (VPD) as it has been recognized as a key variable for dry deposition (Kavassalis and Murphy, 2017; Otero et al., 2018). The VPD was calculated from the corresponding hourly data of air temperature and relative humidity. Moreover, we included the O_3 concentrations from the previous hour (C_{O3} (t-1)) and the MDA8 concentrations from the previous day (C_{MDA8} (t-24)) to represent the persistence of previous chemical conditions, (Pusede et al., 2015). Table 1 provides a summary with the covariates included in the model.

We used a forward selection procedure of the best set of covariates and/or its interactions that maximised the deviance explained. The model improve-ment was assessed with the Akaike Information criterion (AIC) (Akaike, 1974). The selection process, applied individually at each station and period, led for most of the stations to a similar model defined with three interaction terms: 1) temperature and NO_x, 2) VPD and C_{O3} (t-1), and 3) ΔBLH and C_{MDA8} (t-24).

Thus, a GAM with the mentioned form was built for each station and period.

Here, we will refer as GAM-P1 to the GAMs built for first period 1999–2008 and similarly, as GAM-P2 to the GAMs built for the second

Table 1
Summary of the covariates included in the model.

Covariate	Long name	Units	Source
tas	Air surface 2 m temperature	°C	ERA5
NO_x	Nitrogen oxides	µgm^{-3}yr^{-1}	Airbase
C_{O3} (t-1)	Lag of ozone (1 h)	µgm^{-3}yr^{-1}	Airbase
VPD	Vapor pressure deficit	kPa	ERA5
C_{MDA8} (t-24)	Lag of MDA8 (24 h)	µgm^{-3}yr^{-1}	Airbase
ΔBLH	Growth of BLH	%	ERA5

period 2009–2018. The model selection indicated that as variables were added and the model complexity increased (i.e. more interactions), the AIC decreased and the deviance explained increased (Fig. S1). The model performance was assessed through standard diagnostic plots (Wood, 2006): QQ plots of the deviance residuals, scatter plots of the residuals against the fitted values, histogram of residuals and scatter plots the response against the fitted values (Fig. S2). More details about the GAM description and the selection procedure can be found in the supplementary material.

4. Results

4.1. NO$_x$ changes and climate penalty

Before calculating the m$_{O3\ T}$, we assess changes in the NO$_x$ concentrations over the whole period of study (1999–2018). For that, we examine time series of the annual 5th, 50th, and 95th percentiles calculated from daily NO$_x$ concentrations, assessing the trends (Kendall, 1975) and estimating its slope (Sen, 1968; Theil, 1950). Fig. 2 shows annual 5th, 50th, and 95th percentiles calculated from daily NO$_x$ concentrations at some example stations located in Berlin, Rhineland-Palatinate and Saxony that are representative for each station type area and will be used below to present the modelling results. The NO$_x$ concentrations at the 95th percentile have generally declined over the overall period of study (1999–2018), but the most dramatic reduction is observed during the first part ot the period (1999–2008) in the

example stations. Larger decreases are observed at the stations in Rhineland-Palatinate, specially at the urban station (Wörth-Marktplatz, Fig. 1) where the NO$_x$ concentrations at the 95th percentile declined at the rate of -4.45 µgm^{-3}yr^{-1} in the first period 1999–2008 and -3.38 µgm^{-3}yr^{-1} in the second period 2009–2018 (see Fig. S3 in the supplementary material). Similar trends are observed at the urban stations located in the southwestern and central regions (Fig. S3 and S4). The NO$_x$ concentrations at the 95th percentile have been reduced at the urban and rural stations in Berlin during the first period 1999–2008 with decreasing rates of -2.78 and -1.77 µgm^{-3}yr^{-1}, respectively, while small and non significant changes are observed during the second period (Fig. S3). Overall, annual 50th percentile NO$_x$ concentrations show a steady decrease in most of the stations of the study, more pronounced during the first period, and small changes are found at the 5th percentile of NO$_x$ especially during the second period 2009–2018 (Fig. S3 and S4).

As emissions of NO$_x$ generally decrease on weekends, O$_3$ concentrations tend to be higher on weekends compared to O$_3$ concentrations on weekdays in a VOC- limited regime because decreased NO$_x$ increases O$_3$ production (LaFranchi et al., 2011; Murphy et al., 2007; Pusede and Cohen, 2012). This so-called weekend-weekday effect has been widely used to assess the effectiveness of emission con-trols and it provides insights into the O3 regimes (Abeleira and Farmer, 2017). In addition to long-term changes in NOx, we have further examined the weekend-weekday effect separately for each period as the differences between the week-end (Saturday and Sunday) and the weekday (Monday to Friday) of MDA8 concentrations (i.e.
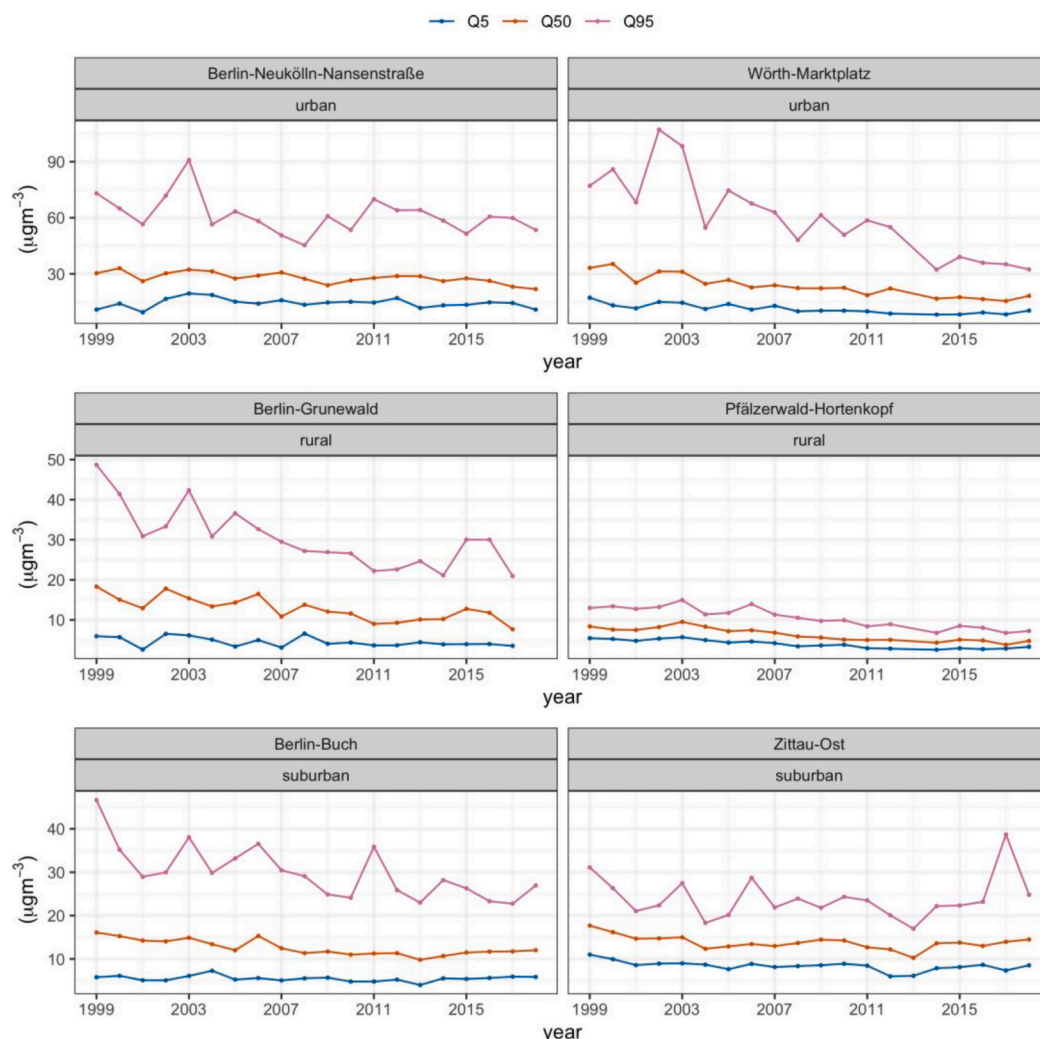

Fig. 2. Time series of annual 5th, 50th, and 95th percentile of NOx concentrations for the whole period of study (1999–2018) at the example stations.

$\Delta(MDA8_{weekend}\text{-}MDA8_{weekday}))$ to elucidate the dominant chemistry regime. A positive weekend-weekday effect is consistent with a VOC-limited system, while a negative weekend-weekday effect is indicative of NO_x-limited system. We have examined the weekend-weekday effect at different temperature regimes, defined based on the percentiles of the temperature dis-tribution: low (< 10th), low-moderate (10-50th), high-moderate (50-90th) and high (>90th) temperatures. We applied the nonparametric Mann-Whitney test to asses the statistical significance ($p < 0.05$) of the weekend-weekday differences at each station and period (Sicard et al., 2020). Fig. 3 shows the weekend-weekday effect for each period and temperature bins. The weekend-weekday effect is strong at low temperatures in both periods (VOC-limited) but it is observed a general significant decreasing weekend-weekday effect at most of the stations during the second period. At low-moderate and high-moderate temperatures the weekend-weekday effect is in general lower in the second period, especially in the southwestern stations that are transitioning to NO_x-limited chemistry. At high temperatures the NO_x-limited regime dominates in both periods. Exceptions are found in some urban stations over the southwestern regions that show a transition from a VOC-limited regime in the first period to a NO_x-limited regime in the second period. On the contrary, during the second period the weekend-weekday effect increases in the northern stations (e.g. Berlin) that depict a VOC-limited chemistry. This analysis indicates that during the first period a VOC-limited chemistry dominated at most of the stations (including some rural stations) at low and moderate temperatures. However, we observe that a large number of stations are transitioning to NO_x-limited chemistry at all temperatures, in which O_3 concentrations tend to decrease due to NO_x reductions. We can anticipate the effectiveness of emissions reductions in those urban stations transitioning to a more NO_x-limited chemistry.

Fig. 4 shows the spatial distribution of the $m_{O3\ T}$ for each period and the changes in the slopes (relative to the first period). The highest values are found in the southwest stations during the first period 1999–2008 with $m_{O3\ T}$ 5–6.5 $\mu gm^{-3}{}^{\circ}C^{-1}$. Among these sites, urban stations show a higher sensitivity to temperature compared to suburban and rural stations. The lowest values of $m_{O3\ T}$ during the first period are observed in the north and eastern stations (4–5, $\mu gm^{-3}{}^{\circ}C^{-1}$). Significant differences between the $m_{O\ T}$ calculated for each period are observed in most of the stations, including some rural areas in the southern regions where the m O T dropped -1.2 $\mu gm{-}3\ ^{\circ}C{-}1$ (Fig. 4, b). Only a few stations show similar values of $m_{O3\ T}$ in both periods (e.g. Berlin). Boleti et al. (2020) reported a general decreasing sensitivity of daily maximum of O_3 with temperature for a shorter period (2000–2015) in regional clusters defined over Europe. They found larger trends in $m_{O3\ T}$ at high and moderate polluted clusters and they argued that it might be due to NO_x reductions. Here, we found a general decrease in $m_{O3\ T}$ obtained from long-term data across different environments (i.e. rural, urban and suburban). Our results also pointed out significant differences in the $m_{O3\ T}$ across stations, with some polluted areas where the $m_{O3\ T}$ did not show significant changes with time (e.g. Berlin). A priori it is not evident what the impact of NO_x reductions is in the O_3 sensitivity to temperature, in particular in rural environments. Therefore, we next examine the variability of ΔO_3 as a function of temperature and NO_x in order to provide further insights into the nonlinear temperature-dependence of NO_x and the potential impacts on the observed $m_{O3\ T}$.

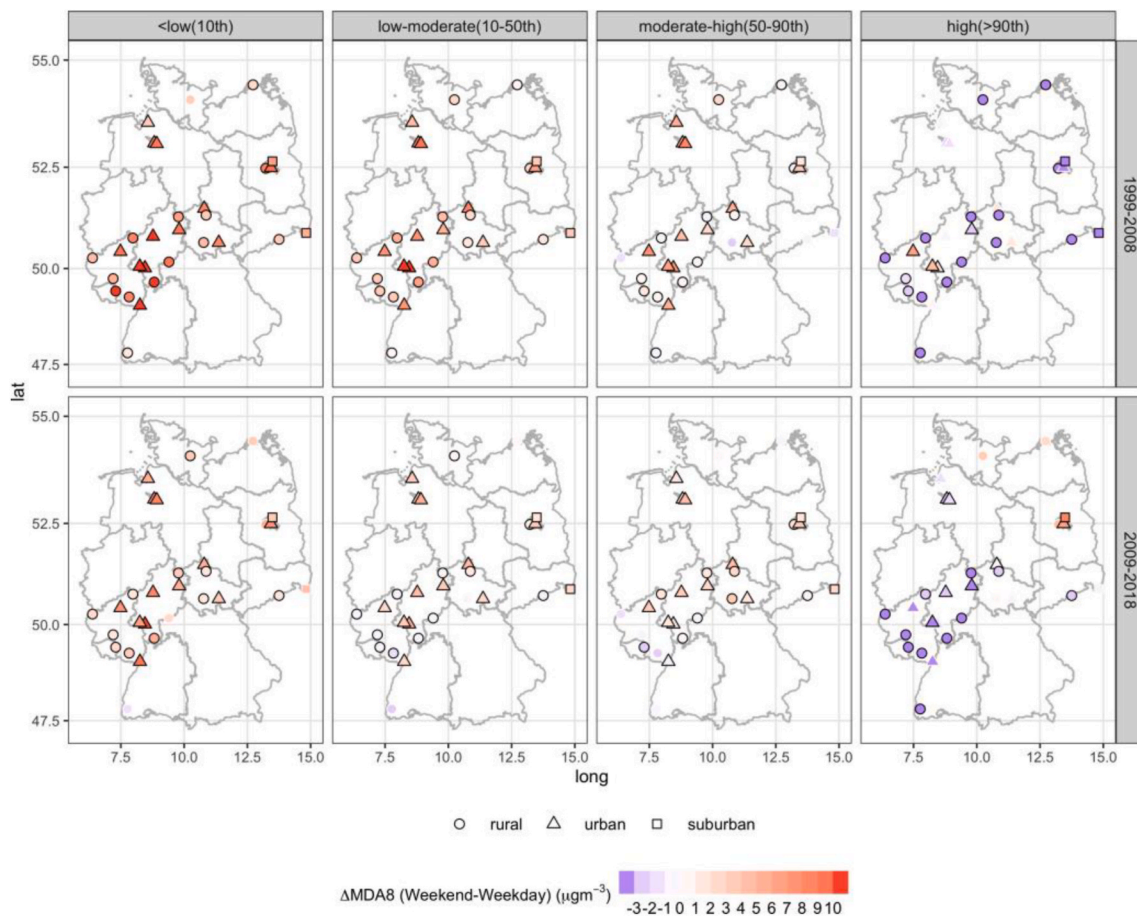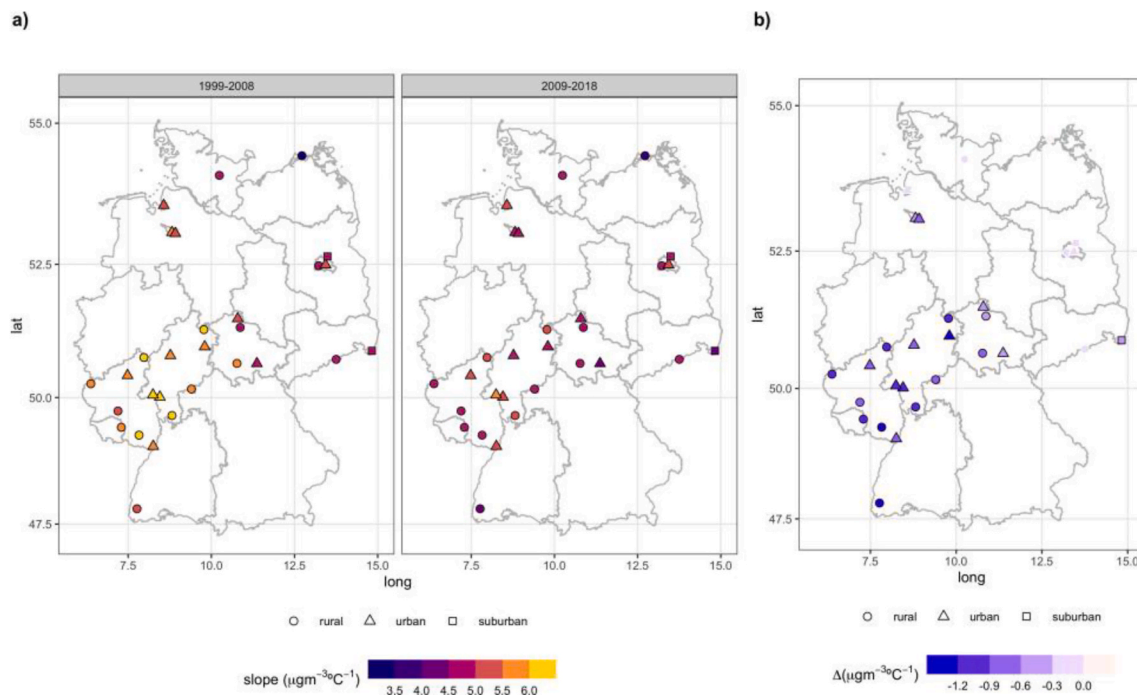**Fig. 3.** Spatial distribution of the weekend-weekday effect calculated for each period and tempertature regime: low (< 10th), low-moderate (10-50th), moderate-high (50-90th) and high (>90th). Black contours indicate stations with statistical significant weekend-weekday differences at the 0.05 significant level.

Fig. 4. Spatial distribution of climate penalty factor calculated at each stations and period. (a) and the changes in the slopes (relative to the first period) (b). In b), black contours indicate stations where differences in the climate penalty are statistically significant at the 0.05 significant level. of the interactions between the selected covariates is better suited for urban and suburban areas than for rural regions.

4.2. Model performance

As mentioned above, the final model obtained from the selection proce-dure includes three interaction terms to represent: 1) photo-chemical processes (temperature-NO_x), 2) dry deposition (VPD-C_{O3} (t-1)), and 3) mixing processes (ΔBLH-C_{MDA8} (t-24).). The performance of the GAMs was assessed by the ad-justed r-squared for the model (R^2), defined as the proportion of the variance explained (Fig. 5). Table S1 in the supplementary material provides the R^2 and the AIC values obtained at each station and period. The results showed simi-lar R^2 values in both periods over most of the stations, with some exceptions where GAM-P1

seem to perform better than GAMP-P2 (e.g. over the region of Hessen). In general, GAMs showed a better performance over urban and suburban stations and ~40% of the ΔO_3 variability was captured. The models performed poorly when applied to rural stations, they showed lower values of R^2. This likely reflects that GAMs designed with the underlying assumptions.

4.3. Model interactions

Our approach is built upon a conceptual model (3) to evaluate the effect of chemical, deposition and dynamical-mixing processes affecting
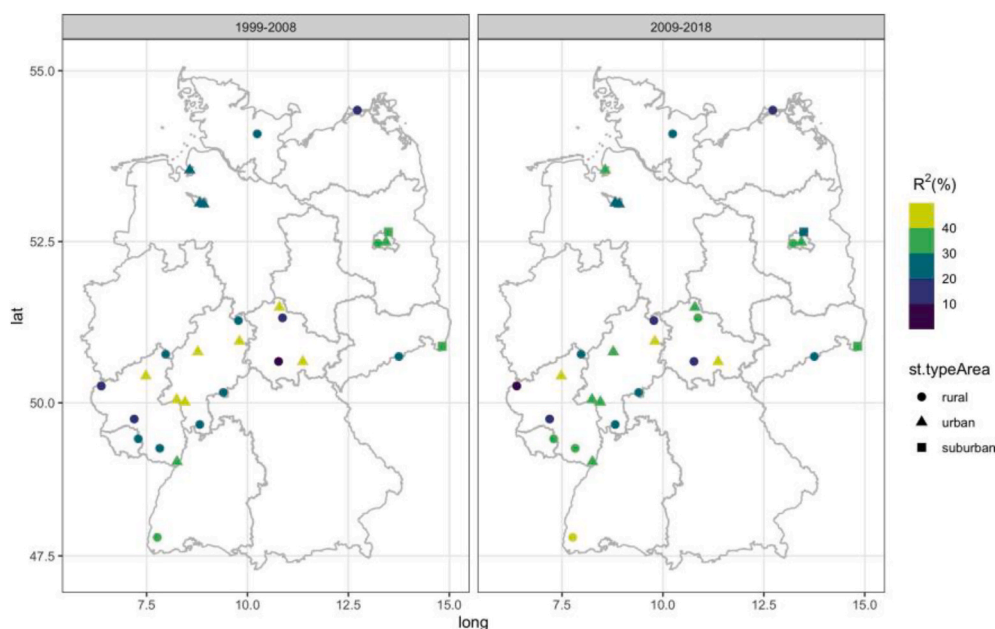
Fig. 5. Spatial distribution of the adjusted r-squared, R^2, for GAM-P1 (left) and GAM-P2 (right).

the O$_3$ production. Given that ΔO$_3$ is modelled with GAMs separately at each station and period, a large number of interaction surfaces were obtained. Thus, we focus on a representative number of stations for each station type area (i.e. rural, urban and suburban). The example stations presented here were selected based on a relatively good performance of the model as well as the corresponding geographical location in order to examine the results from the previous section showing marked differences in the sensitivity of MDA8 to temperature. Figures showing the results obtained for the rest of stations are available in the supplementary material. Note that the contour plots presented below reflect the partial effects, which allow us to compare the effect of those covariates included in the interaction term without considering the intercept and the other covariates (e.g. Fig. 6). The summed effects that include the intercept and constant values for the others covariates not shown in the interaction surface, presented similar shapes but with the additive effect of those constant values (not shown). To estimate the predicted surfaces within a range of data sufficiently supported by the observations, we used the first and the third quantile of the distribution of the corresponding covariates for each station type area (urban, rural and suburban).

4.3.1. NO$_x$ and temperature

Fig. 6 shows ΔO$_3$ as a function of NO$_x$ concentrations and temperature for the example urban stations located in Berlin (Berlin-Neukölln-Nansenstraße) and in Rhineland-Palatinate (Wörth-Marktplatz) (see Fig. 1). Also shown in Fig. 6 are the estimated regression lines for temperature while holding constant NO$_x$ concentrations (i.e. mean conditions of NO$_x$ each period). As we aim to assess the impact of NO$_x$ reductions in the O$_3$-temperature relationship, we also use the GAM-P1 to project the ΔO$_3$ response to temperature, as it has been estimated under the first period conditions, but using the mean NO$_x$ concentrations of the second period 2009–2018. We predict ΔO$_3$ estimates for the second period 2009–2018 (i.e. NO$_x$ conditions) using the GAM-P1 parameters. Examining the GAM-P1 projection for the second period 2009–2018 and the GAM-P2 estimations can provide useful insight into the changes in the ΔO$_3$ sensitivity to temperature when lowering NO$_x$ concentrations.

The interaction surfaces obtained from both stations illustrate the temperature dependence of ΔO$_3$ with increasing temperatures (Fig. 6, left). The temper-ature dependence of ΔO$_3$ is observed to vary with NO$_x$, but also with tem-perature in both stations. In Rhineland-Palatinate it can be noted that the regime change from VOC to NO$_x$-limited chemistry, in which ΔO$_3$ effectively decreases lowering NO$_x$ concentrations, occurs at lower NO$_x$ in the second period 2009–2018 compared to the first period 1999–2008 (Fig. 6). For example, the transition to NO$_x$-limited chemistry at higher temperatures (>23 °C) occurs at lower values of NO$_x$ (14 μgm^{-3}) for the second period compared to the transition observed during the first period (20 μgm^{-3}) for similar temperatures. On the contrary, the VOC-limited regime observed in Berlin is generally dominant, ΔO$_3$ decreases with increasing NO$_x$ especially during the first period. In the second period the contours reveal a small region of NO$_x$-limited chemistry, but only when NO$_x$ ranges between 20 and 30 μgm^{-3} for the highest temperatures (25 °C). These results are consistent with the decreasing weekend-weekday effect observed at Rhineland-Palatinate for the second period, but not found in Berlin (see Fig. 3), which indicates that emission reductions over time were more effective in Rhineland-Palatinate (e.g. in Rhineland-Palatinate NO$_x$ declined by 35%, while in Berlin NO$_x$ declined only by 7.5% in the second period). We examine the ΔO$_3$ response to temperature under the mean NO$_x$ conditions for each period using GAM-P1 and GAM-P2 along with the prediction obtained from GAM-P1 that projects the ΔO$_3$ response in the second period 2009–2018 (prediction line in Fig. 6, right). This analysis is aimed to assess.

Whether the shapes of the regression lines that represent the relationship ΔO$_3$- temperature change when comparing the periods. If the shapes from the projected GAM-P1 and GAM-P2 differ, we interpret that changes in NO$_x$ are not enough to explain the observed changes in the ΔO$_3$-temperature relationship.

In Berlin, the ΔO$_3$ response to temperature shows a similar increase with tem-perature in both periods. In this case, the GAM-P1 prediction for the second period 2009–2018 is in a good agreement with the shape obtained from GAM- P2, which suggest that a decreasing temperature sensitivity of ΔO$_3$ could be explained by NO$_x$ reductions. The increase of ΔO$_3$ with temperature is also depicted in Rhineland-Palatinate. But, in Rhineland-Palatinate the prediction from GAM-P1 for the second period 2009–2018 reveals discrepancies at higher temperatures when
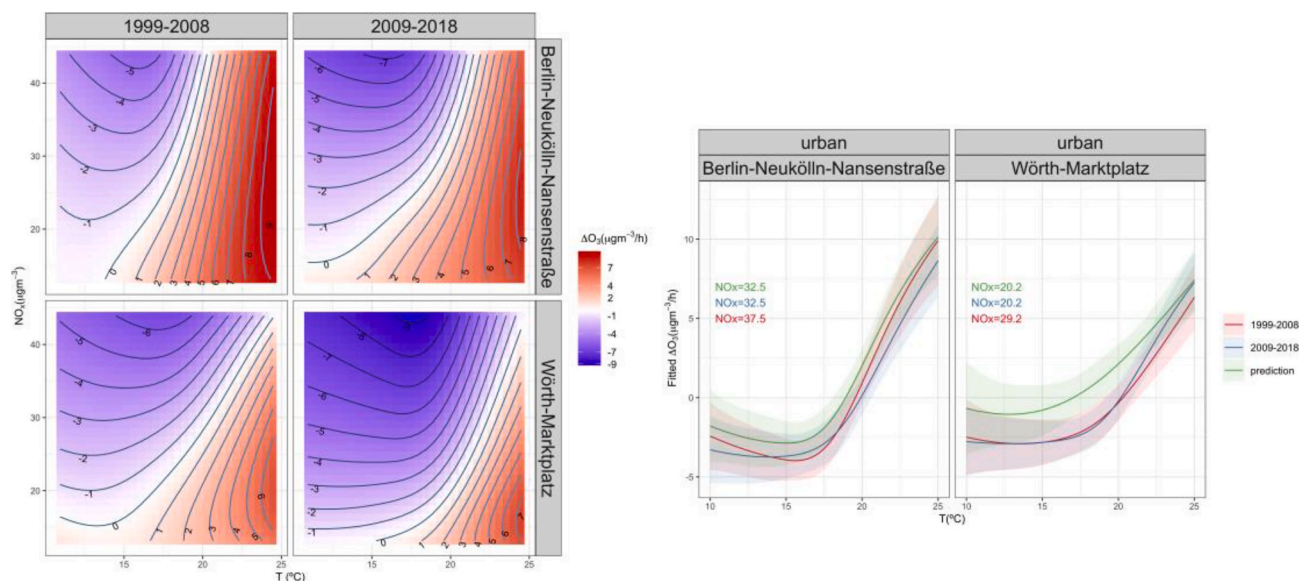
Fig. 6. Contour plot for the interaction temperature^{-}^{NO}x at the urban stations in Berlin (Berlin-Neukölln-Nansenstraße) and Rhineland-Palatinate (Wörth-Marktplatz) for the first period 1999–2008 and second period 2009–2018 (left). In the right panel, smooth functions representing the temperature response of O$_3$ production rates under mean conditions of NOx (indicated by the text numbers) obtained from GAM-P1 (red line) and GAM-P2 (blue line), along with the prediction of the O$_3$ response using GAM-P1 (green line). Shaded bands represent the pointwise 95% confidence interval. . (For interpretation of the references to colour in this figure legend, the reader is referred to the Web version of this article.)

comparing to the ΔO_3 response from GAM-P2. It can be noted that the prediction from GAM-P1 for the second period (prediction line, Fig. 6) does not capture the steepness at temperatures above 20 °C showed by GAM-P2. Contrasting to the results in Berlin, the changes in the shape that represents the ΔO_3 as a function of temperature suggest that the NO_x reductions would only partially explain the observed changes in the O_3-temperature relationship, but rather an underlying effect is likely to influence the ΔO_3 at higher temperatures. We interpret that the changes in the shapes would indicate effective reductions of VOCs over time that played a significant role on controlling ΔO_3.

We found similar features in the rest of the urban stations than in the example stations, with consistent interaction surfaces in terms of the ΔO_3 response to NO_x and the temperature dependence (Fig. S5). As in Rhineland-Palatinate, the regression lines were slightly different when comparing GAM-P2 and the projected ΔO_3 response under NO_x reductions (Fig. S6), which reinforce our hypothesis of an underlying factor influencing the ΔO_3-temperature relationship.

We further assess the effect of the temperature and NO_x on ΔO_3 separately with GAM-P1 and GAM-P2 under fixed NO_x and temperature conditions determined as the 10th, 50th and 90th percentiles of the corresponding distributions.

Over the whole period of study (1999–2018). In contrast to the contour plots (Fig. 6), we now include the intercept and a constant value (i.e. median) for the rest of the covariates, in order to further examine the summed effects. Table 2 summarizes the values of the covariates for the selected urban stations. The shaded areas denote the 95% pointwise confidence intervals of the GAM estimates. It should be noted that the smooth functions show a major uncertainty in the regions with less data (i.e. in the tails of the presented ranges). Fig. 7 shows ΔO_3 as a function of temperature. ΔO_3 estimates are generally lower in the second period 2009–2018 under moderate (50th) and high (90th) NO_x concentrations for moderate temperatures (e.g. 20 °C) at both stations. It can be observed the decreasing temperature dependence of ΔO_3, especially for high NO_x concentrations during the second period. Similarly, Fig. 8 illustrates the changes in the nonlinear relationship between ΔO_3 and NO_x. In general, at lower temperatures (10th) ΔO_3 decreases with increasing NO_x concentrations (VOC-limited), while it increases with increasing NO_x at high temperatures (90th) (NO_x-limited). We found that during the second period the regime change (i.e. to a NO_x-limited regime) occurs earlier at lower NO_x for high temperatures, particularly in Rhineland-Palatinate. In Berlin, the relationships are similar for both periods, but showing lower ΔO_3 estimates in the second period. At moderate temperatures (50th) only Rhineland-Palatinate shows peak ozone production and therefore a transition towards NO_x-limited chemistry during the second period. Such transition is not observed in the first period due to higher NO_x concentrations. Consistent with Fig. 6, in Berlin the regime transition during the second period is not observed as a result of high.

We observed a shift of the ΔO_3 peak towards lower NO_x concentrations at most of the urban stations during the second period, which indicates that those sites are near to a more NO_x-limited regime as a result continued reductions of NO_x and concurrent VOC decreases. Ultimately, we infer effective VOC. reductions that led to ΔO_3 decreases during the second period.

Fig. 9 depicts the interaction surfaces for two selected rural stations located in the same regions than the urban stations presented above,

Berlin (Berlin-Grunewald) and Rhineland-Palatinate (Pfälzerwald-Hortenkopf). The temperature dependence of ΔO_3 is stronger in the first period 1999–2008 compared to second period 2009–2018. The GAMs-P2 show a decreasing sensitivity of ΔO_3 to temperature and ΔO_3 is generally lower with increasing temperature under similar conditions of NO_x. We see similarities between the rural and urban stations in Berlin, in terms of the shape of the nonlinear relationship between temperature and NO_x, which is expected due to the proximity between both stations (Fig. 1). It must be noted that the Berlin-Grunewald has been categorised as a rural-near-city in the latest version of the Airbase dataset. In Berlin the regimes transition with temperatures is well observed in both periods: a NO_x-limited chemistry at higher temperatures and a VOC-limited chemistry at lower temperatures. We observed that at similar NO_x concentrations during the second period, ΔO_3 tends to decrease in the NO_x-limited regime (high temperatures) when comparing to the first period, while ΔO_3 increases in the VOC-limited regime (low temperatures). This suggests that NO_x reductions in the rural station of Berlin (declining by 28.8%) led to ΔO_3 decreases at higher temperatures in the second period. In Rhineland-Palatinate, the peak of ΔO_3 occurs at lower NO_x concentrations (< 8 µgm^{-3}) in the second period than the peak observed in the first period (> 8 µgm^{-3}), due to NO_x reductions (declining by 37%). The ΔO_3 as a function of temperature under NO_x mean conditions is also shown in Fig. 9 (right). For both rural stations, the shapes of the regression lines obtained from the GAM-P2 and the projected ΔO_3 response from GAM-P1 are different. In Rhineland-Palatinate the temperature dependence is considerably lower than in Berlin and a flat regression line is shown by GAM-P2 for the second period. The discrepancies found here point out that changes in VOCs have also influenced ΔO_3. This is consistent with a dominant VOC-limited chemistry at low and moderate temperatures found for most of the stations during the first period, including rural stations (see Fig. 3), where changes in organic reactivity would have had a major influence. Overall, we found a larger variability among the rest of the rural stations considered in the study, in terms of the interaction surfaces NO_x-temperature (Fig. S7). The results show a decreasing temperature dependence of ΔO_3 during the second period at higher temperatures in some stations. This is also reflected in the estimated temperature response of ΔO_3 when comparing GAM-P2 and the projected response using GAM-P1 (Fig. S8).

As shown in Fig. 9 it can be observed the differences in the shapes of the regression lines when comparing both periods. This is reflected when examining the ΔO_3 response as a function of temperature under low (10th), medium (50th) and high (90th) levels of NO_x (Fig. S9). Such differences between the periods are more evident in Rhineland-Palatinate where the regression line corresponding to the second period 2009–2018 becomes flat at temperatures between 18 and 22 °C at moderate (50th) and high (90th) NO_x concentrations. In Berlin, ΔO_3 slightly decreases in the second period, and the regression lines are very similar at the fixed NO_x conditions in both periods. The variations of ΔO_3 with NO_x at different temperature conditions indicates a major decrease of ΔO_3 at moderate (50th) and high (90th) temperatures in the second period in Rhineland-Palatinate than in Berlin. Little changes of ΔO_3 with NO_x are observed at low temperatures (Fig. S10).

Only two suburban stations were included in this study, in Berlin and in Saxony (see Fig. 1), both eastward located. The contours obtained in each period and station showed similar patterns than those found for

Table 2
Median values of the covariates during the period first 1999–2008, and second period 2009–2018 for the example urban stations. Note that these values are obtained from the input data used for the GAMS (i.e. previously filtered).

Code	Station name	Period	NOx	tas	ΔBLH	VPD	CO3 (t-1)	^{c}MDA8$^{(t-24)}$	type
DEBE034	Berlin-Neukölln-Nansenstraße	1999–2008	28.00	17.71	22.65	0.39	42.50	76.12	urban
DEBE034	Berlin-Neukölln-Nansenstraße	2009–2018	24.26	18.41	23.36	0.46	48.84	79.11	urban
DERP025	Wörth-Marktplatz	1999–2008	21.07	18.82	24.13	0.53	52.00	90.12	urban
DERP025	Wörth-Marktplatz	2009–2018	15.23	19.00	24.67	0.56	51.28	85.46	urban
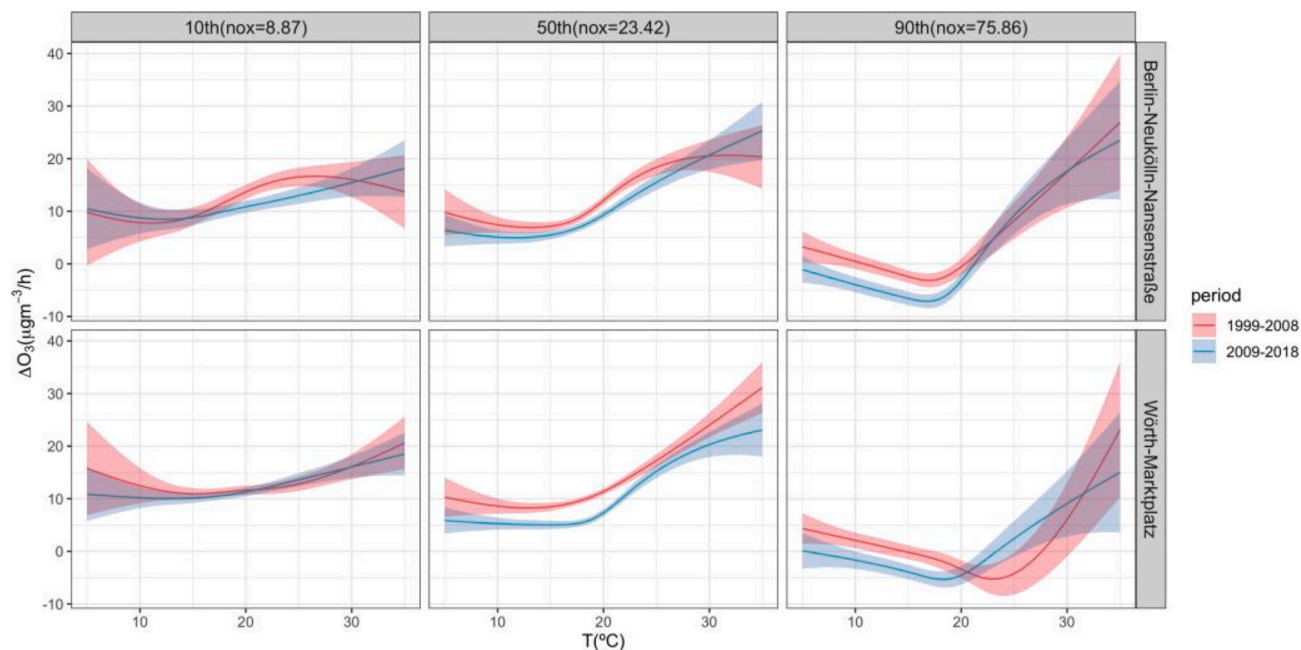
Fig. 7. Smooth functions for temperature at low (10th), medium (50th) and high (90th). NO_x conditions, which are detailed in each corresponding title. Shaded bands represent the pointwise 95% confidence interval. NO x concentrations at such temperatures (50th).
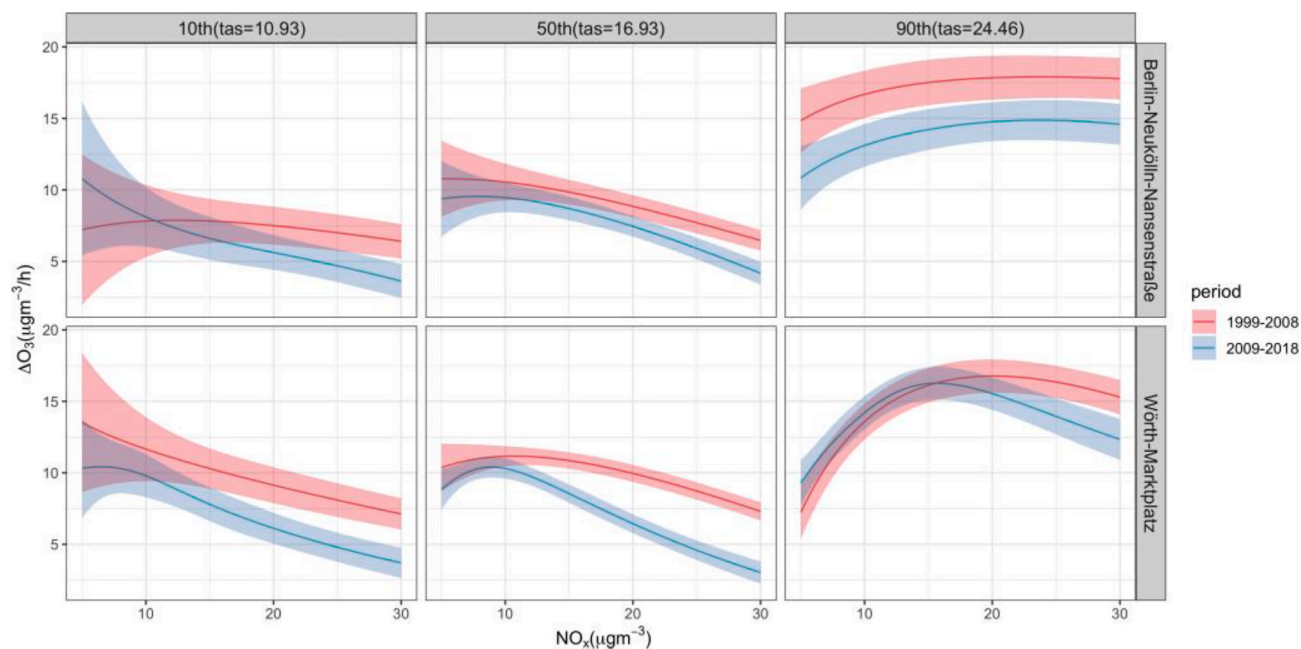
Fig. 8. Smooth functions for NOx at low (10th), medium (50th) and high (90th) temper-ature conditions, which are detailed in each corresponding title. Shaded bands represent the pointwise 95% confidence interval.

urban stations, especially in Berlin. The GAMs consistently reproduce the temperature dependence of ΔO_3 at higher temperatures and the differences between the GAM-P2 and the projected ΔO_3 response to temperature with GAM-P1 were more evident in Saxony (not shown).

4.3.2. VPD and O_3 from the previous hour (C_{O3} (t-1))

We discuss now the interaction term from VPD and C_{O3} (t-1). VPD is crucial and controls the stomatal conductance. Its effects can be summarised as follows: under high VPD levels (associated with high temperatures), plants cannot extract sufficient moisture from dry soils to satisfy the atmospheric demand for evapotranspiration (Teuling, 2018).

In this situation of drought stress, plants close their stomata to reduce water loss and limit the uptake of ozone by vegetation.

Fig. 10 reveals the nonlinear relationship between VPD and the C_{O3} (t-1) at the selected urban stations in Berlin and in Rhineland-Palatinate. In general, ΔO_3 tends to increase with higher levels of VPD (i.e. drier conditions) and low O_3 concentrations from the previous hour in both locations and periods. In the first period, the contribution of the inter-action between VPD and persistent O_3 concentrations is similar at both locations, and the model shows maximum ΔO_3 at C_O (t-1) < 30 μgm^{-3} and VPD > 0.70 kPa. In Berlin, the results ob- 3 tained from GAM-P2 suggest that higher levels of VPD and low C_{O3} (t-1) ($\sim$ 30 μgm^{-3}) lead
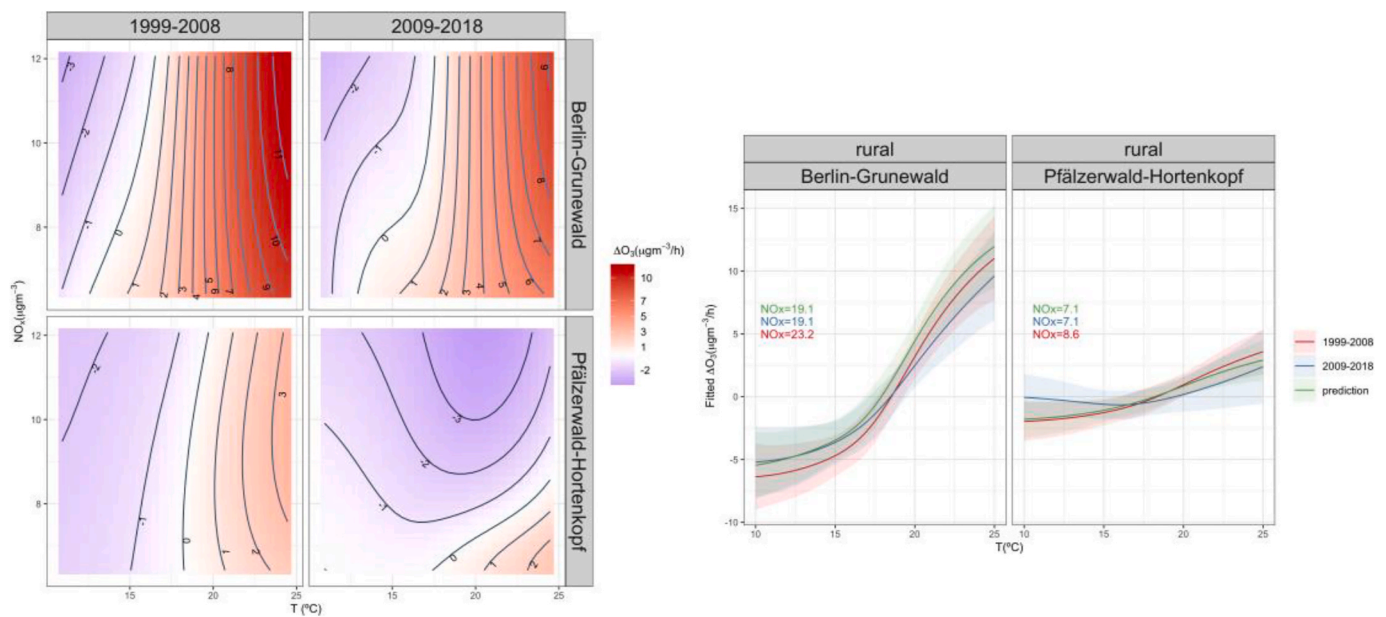
Fig. 9. Contour plot for the interaction temperature-NOx at the rural stations in Berlin (Berlin-Grunewald) and Rhineland-Palatinate (Pfälzerwald-Hortenkopf) for the first period 1999–2008 and second period 2009–2018 (left). In the right panel, smooth functions represent-ing the temperature response of O3 production rates under mean conditions of NOx (indicated by the text numbers) obtained from GAM-P1 (red line) and GAM-P2 (blue line), along with the prediction of the O3 response using GAM-P1 (green line). Shaded bands represent the pointwise 95% confidence interval. . (For interpretation of the references to colour in this figure legend, the reader is referred to the Web version of this article.)
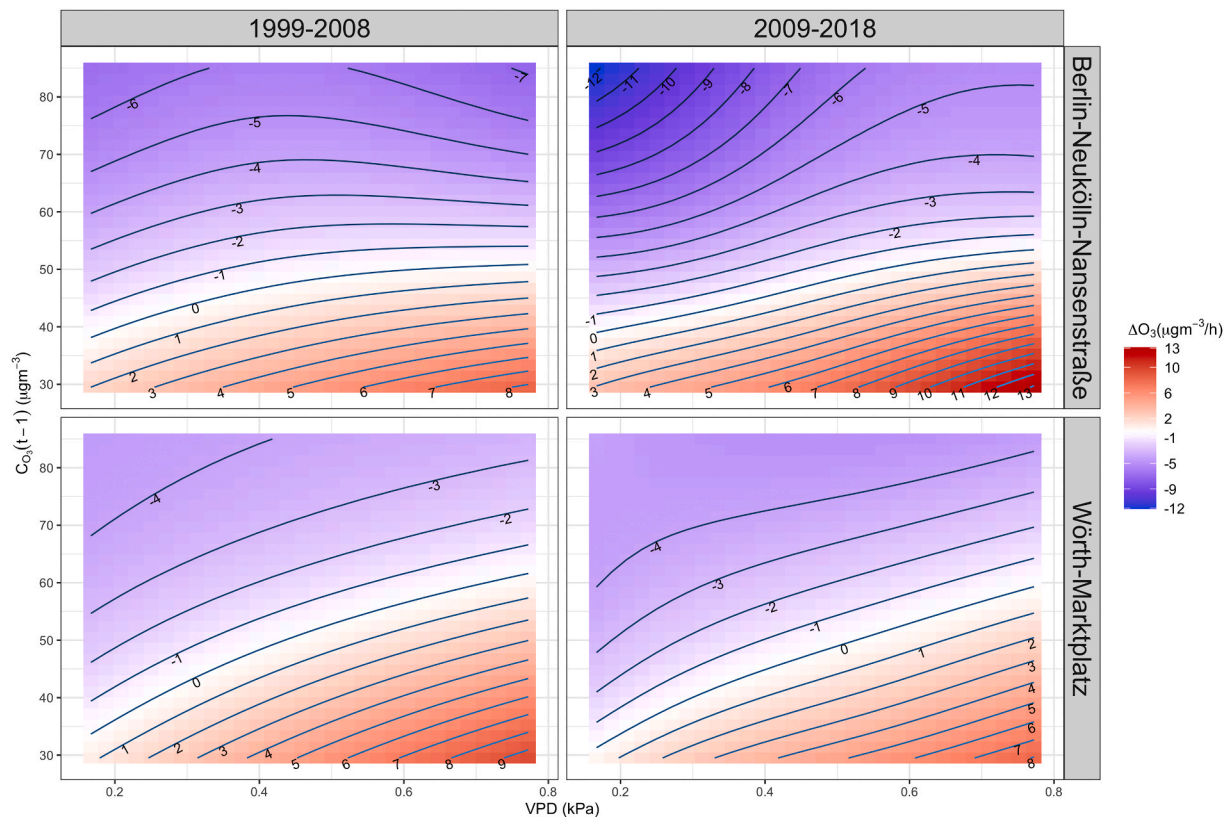
Fig. 10. Contour plot for the interaction VPD-CO3 (t − 1) at the urban stations in Berlin (Berlin-Neukölln-Nansenstraße) and Rhineland-Palatinate (Ẅorth-Marktplatz) for the first. period 1999–2008 and second period 2009–2018.

to an increase of ΔO_3, but the ΔO_3 tends to decrease faster with high C_O (t-1) concentrations (above 50 μgm^{-3}) when comparing to GAM-P1. The interaction surfaces obtained in Rhineland-Palatinate show small

changes 3 when comparing both periods.

In the case of the rural stations, we see large differences among the stations (Fig. S11). ΔO_3 dependence with VPD is more pronounced in

Rhineland- Palatinate, especially in the second period 2009–2018 with a larger increase of ΔO_3 with increasing VPD levels (i.e. drier conditions). In this case, GAM- P1 shows little changes in the estimated ΔO_3 (~ 3 μgm^{-3}) at low C_O (t-1) concentrations for all range of VPD, while the GAM-P2 shows a significant 3increase of ΔO_3 under similar C_{O3} (t-1) concentrations when moving to higher VPD. In Berlin, C_{O3} (t-1) concentrations seems to have a major influence on ΔO_3, and ΔO_3 estimates are slightly lower in the second period 2009–2018 than in the first period 1999–2008. The interaction between VPD and C_{O3} (t-1) in the suburban stations (Berlin and Saxony) is consistent with the patterns found in the urban and rural stations and ΔO_3 increases with higher VPD and low C_{O3} (t-1) concentrations (not shown).

Our results illustrate that the combination of high VPD and lower C_{O3} (t-1) concentrations result in higher ΔO_3 (thus, less uptake of O_3). Moreover, given that O_3 concentrations are typically lower in urban environments due to the local scavenge of O_3 (NO titration), a larger contribution of the interaction of VPD and C_{O3} (t-1) to ΔO_3 in the urban and suburban stations than in the rural stations is expected.

### 4.3.3. ΔBLH and MDA8 from the previous day ($C_{MDA8}(t-24)$)

The effect of mixing processes was introduced in the GAMs through the ΔBLH and C_{MDA8} (t-24). Fig. 11 depicts the interaction surfaces between the covariates ΔBLH and C_{MDA8} (t-24) at the selected urban stations in Berlin and Rhineland-Palatinate. In general, ΔO_3 is mainly dependent on changes in ΔBLH and it increases at higher ΔBLH, while the influence of C_{MDA8} (t- 24) on ΔO_3 is negligible for $\Delta BLH\, sim < 30\%$. The results obtained from most of the stations at different environments (i.e. urban, rural and suburban) showed consistent shapes with the patterns described for the selected stations (not shown).

These interaction surfaces can be used to interpret the nonlinear relation-ship between ΔBLH and C_{MDA8} (t-24) concentrations. As BLH grows, air is. entrained from layers aloft and O_3 production rates can increase or decrease depending on the O_3 concentrations in this residual

layer (Haman et al., 2014). We show that a rapid development of the BLH along with high C_{MDA8} (t-24) (from the previous day), likely stored at the residual layer, lead to an increase of ΔO_3. Note that C_{MDA8} (t-24) concentrations seems to have an influence on ΔO_3 when the BLH rapidly changes. These results are consistent with previous studies that showed the importance of O_3 persistence for high O_3 levels (Otero et al., 2016). The effect of this interaction was slightly larger in most of the ur-ban and suburban stations as compared to the rural stations (not shown), while small differences are observed when comparing the patterns obtained from each period.

5. Discussion

Despite substantial reductions of emission of O_3 precursors achieved over the past decades, high O_3 levels still remain a concern in Europe (EEA, 2019, 2020). While several studies showed a decreasing climate penalty of O_3 as a result of emission controls (Bloomer et al., 2009; Lin et al., 2020; Boleti et al., 2020), due to its strong temperature dependence, further emissions controls might be required as the climate penalty can be aggravated under a warmer climate (Jing et al., 2017; Lin et al., 2020). Our study provides a comprehensive observational-based analysis of the O_3 sensitivity to temperature and how NO_x reductions have influenced the observed changes of the O_3-temperature relationship. We focused on Germany where temperature is a key driving factor of O_3 in summertime (Otero et al., 2018). A total of 29 stations were selected for the period 1999–2018, which was further divided in two 10-year periods (1999–2008, 2009–2018). While the period selection was mainly limited by the availability of co-located data of both O_3 and NO_x, the subdivision of a 10-year period allowed us to asses the impact emissions controls on the temperature dependence of O_3. Moreover, as observed changes of local O_3 behaviour in a 10-year period are likely driven by short-term emission reductions of its precursors (NO_x and VOCs) (Wolff et al., 2013; Sicard et al., 2020), our approach provides
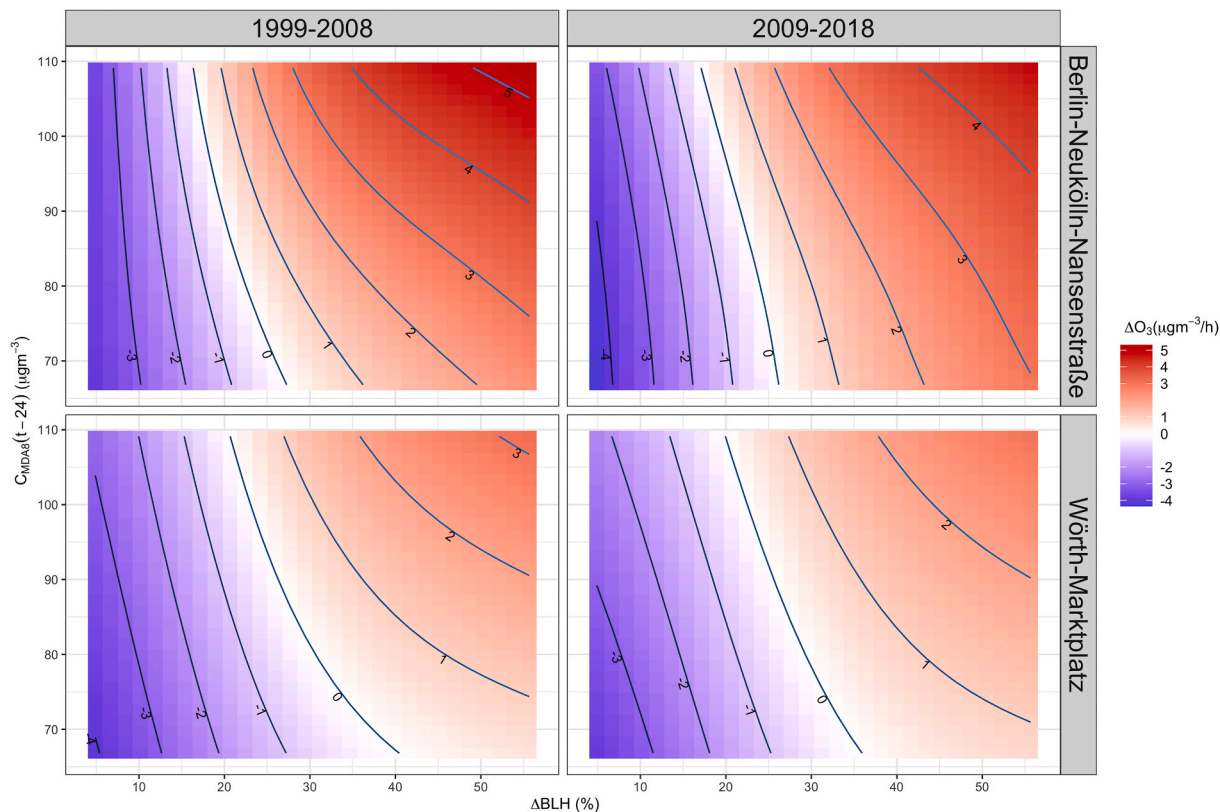
Fig. 11. Contour plot for the interaction ΔBLH-CMDA8 (t − 24) at the urban stations in Berlin (Berlin-Neukölln-Nansenstraße) and Rhineland-Palatinate (Wörth-Marktplatz) for the first period 1999–2008 and second period 2009–2018.

further insights into the effectiveness of emissions control for mitigating the climate penalty.

We found a general downward trend of the 95th percentile of NO_x concen-trations during the complete period of study, with the most dramatic decrease during the first decade (1999–2008). In contrast, no clear and flat trends were observed in the 50th and 5th percentiles of NO_x over the whole period of study. Consistent with previous work, we saw a decreasing sensitivity of O_3 to temper-ature over time, coinciding with decreasing trends in high NO_x concentrations. A wide number of studies showed that changes in the weekend-weekday effect can explain the transition between O_3 regimes (de Foy et al., 2020; Sicard et al., 2020; Abeleira and Farmer, 2017). Our results showed a weaker weekend-weekday effect during the second period, especially at moderate temperatures (Fig. 3).

While at higher temperatures most of the stations showed a dominant NO_x-limited regime in both periods, we found some exceptions (e.g. Berlin) with an increase of the weekend-weekday effect during the second period, suggesting that stronger control strategies should be required there. In contrast with most of previous studies that analysed O_3 production (Pusede et al., 2014; Coates et al., 2016; Romer et al., 2018), we proposed a simplified statistical modelling framework based on Generalized Additive Models (GAMs) to model the daily increase in O_3 concentrations as a function of three interaction terms accounting for photochemical production (dependent on NO_x and temperature), dry deposition (dependent on vapor pressure deficit and ozone concentrations from the previous hour) and mixing processes (dependent on the boundary layer height growth rate, and ozone concentrations from the previous day.

In most of the stations, the effect of the interaction term NO_x-temperature was larger in the first period than in the second period, resulting in higher ΔO_3 estimates in 1999–2008 compared to ΔO_3 estimates in 2009–2018. A de-creasing sensitivity of ΔO_3 to temperature was shown by the GAMs built for the second period 2009–2018 when comparing with the GAMs from the first period 1999–2008, leading to lower ΔO_3 values under moderate-high tempera-tures in the second period. This decreasing temperature sensitivity was more pronounced in the southward urban stations (e.g. Rhineland-Palatinate). More-over, we found that in a large number of stations the peak of ΔO_3 shift to lower NO_x concentrations in the second period, which indicates the transition to NO_x-limited chemistry, consistent with a weaker weekend-weekday effect showed in second period, in particular at moderate and high temperatures. The observed decreasing trend in the climate penalty over the southwestern stations indicates that NO_x reductions were more effective in decreasing the temperature sensitivity of O_3 at higher temperatures. This was not the case for some of the stations (e.g. Berlin) were the climate penalty did not show significant changes over time.

Using the GAMs derived from the first period 1999–2008 to project the ΔO_3 response to temperature under the mean NO_x conditions of the second period 2009–2018, we showed that the shape of the regression lines have changed in the second period for a large number of urban stations, pointing out the con-tribution of emissions from VOC that also influence ΔO_3. Similar conclusions were obtained for most of the rural stations, where the shape of the projected ΔO_3 response with tempera-ture in the second period 2009–2018 differ from the estimated ΔO_3 response from the GAMs built for that period.

The temperature-dependence of biogenic VOC emissions is well-known. In particular, biogenic isoprene emissions have a strong tem-perature dependence with critical implications on O_3 production, mostly during warmer summer days. Therefore, one plausible explanation for the changes in the shapes of the ΔO_3-temperature relationship might be attributed to the accompanying effect of changes in biogenic emissions (along with NO_x) that are likely influencing the temperature-dependence of ΔO_3 and consequently the $m_{O_3\ T}$. We have shown a general decrease of ΔO_3 at higher temperatures, which may suggest that enhanced temperature-driven biogenic emissions can result in ΔO_3 being more dependent of NO_x (NO_x-limited) and thus, more sensitive to

the NO_x controls. Our results have important implications for the implementation of mitigation strategies, specially when considering the effects of a warming climate. We expect that the methodology described herein can be applied to other locations with available long-term mea-surements to assess how NO_x reductions have influenced the tempera-ture dependence of O_3. Consistent with previous work, we may anticipate that our approach will show changes in the climate penalty factor as well as in the sensitivity of ΔO_3 with temperature. Further analysis to examine in more detail the effect of NO_x reductions in particular locations should be required.

6. Conclusions

We conclude that the emissions controls of O_3 precursors have been generally effective at a large number of the stations used in this study that showed a tendency to move to a NO_x-limited chemistry with time.

While our results point out effective reductions of NOx and VOCs that led to a decreasing O3 sensitivity to temperature, they suggest that further emissions controls, likely targeting VOCs due a dominant VOC-limited regime (e.g. Figs. 3 and 6), should be applied in a few stations of the study to counteract the O_3 climate penalty.

In summary, the sensitivity of O_3 to temperature has decreased during the last period (2009–2018) over a great number of the German stations considered in the study, including rural areas. Even though NO_x reductions accomplished during the last decades have partially coun-teracted the O_3 climate penalty, our study highlights the relevance of considering the influence of additional factors controlling the O_3-tem-perature relationship. Since observations of long-term dataset of VOCs are lacking, further analysis including short-term measure-ments of a suite of VOCs would be definitively required to quantify their con-tribution to the observed changes in the climate penalty.

Data availability

Observational ozone data used in this study are available at the Airbase database of the European Environment Agency (EEA) data ser-vice: https://www.eea.europa.eu/data-and-maps/data/aqereporting-8.

The ERA5 reanalysis products are available on the Climate Data Store (CDS) cloud server: https://cds.climate.copernicus.eu.

CRediT authorship contribution statement

Noelia Otero: Investigation, Methodology, Software, Data curation, Writing – original draft. **Henning W. Rust:** Methodology, Writing – review & editing. **Tim Butler:** Conceptualization, Supervision, Writing – review & editing.

Declaration of competing interest

The authors declare that they have no known competing financial interests or personal relationships that could have appeared to influence the work reported in this paper.

Acknowledgements

Appendix A. Supplementary data

Supplementary data to this article can be found online at https://doi.org/10.1016/j.atmosenv.2021.118334.

References

Abeleira, A., Farmer, D.K., 2017. Summer ozone in the northern front range metropolitan area: weekend–weekday effects, temperature dependences, and the impact of drought. Atmos. Chem. Phys. 17, 6517–6529. https://doi.org/10.5194/hacp-17-6517-2017.

Akaike, H., 1974. A new look at the statistical model identification. IEEE T. Automat. Contr., AC-19 716–723.

Barmpadimos, I., Hueglin, C., Keller, J., Henne, S., Prévôt, A., 2011. Influence of meteorology on pm10 trends and variability in Switzerland from 1991 to 2008. Atmos. Chem. Phys. 11, 1813–1835. https://doi.org/10.5194/acp-11-1813-2011.

Bloomer, B., Stehr, J., Piety, C., Salawitch, R., Dickerson, R., 2009. Ob- served relationships of ozone air pollution with temperature and emissions. Geophys. Rep. 36, L09803.

Bloomer, B., Vinnikov, K., Dickerson, R., 2010. Changes in seasonal and diurnal cycles of ozone and temperature in the eastern u.s. Atmos. Environ. 44, 2543–2551. https://doi.org/10.1016/j.atmosenv.2010.04.031.

Boleti, E., Hueglin, C., Takahama, S., 2019. Trends of surface maxi- mum ozone concentrations in Switzerland based on meteorological adjustment for the period 1990–2014. Atmos. Environ. 213, 326–336. https://doi.org/10.1016/j.atmosenv.2019.05.018.

Boleti, E., Hueglin, C., Grange, S., Prévôt, A., Takahama, S., 2020. Tempo- ral and spatial analysis of ozone concentrations in europe based on timescale decomposition and a multi-clustering approach. Atmos. Chem. Phys. Discuss. https://doi.org/10.5194/acp-2019-909.

Butler, T., Lupascu, A., Nalam, A., 2020. Attribution of ground-level ozone to anthropogenic and natural sources of nitrogen oxides and reactive carbon in a global chemical transport model. Atmos. Chem. Phys. 20, 10707–10731. https://doi.org/10.5194/acp-20-10707-2020.

Carslaw, D., Beevers, S., Tate, J., 2007. Modelling and assessing trends in traffic related emissions using a generalized additive modelling approach. Atmos. Environ. 41, 5289–5299. https://doi.org/10.1016/j.atmosenv.2007.

Chang, K., Petropavlovskikh, I., Cooper, O., Schultz, M., Wang, T., 2017. Regional trend analysis of surface ozone observations from monitoring net- works in eastern north america, europe and east asia. Elementa 5, 1–22. https://doi.org/10.1525/elementa.243.

Coates, J., Mar, K., Ojha, N., Butler, T., 2016. The influence of tem- perature on ozone production under varying nox conditions–a modelling study. Atmos. Chem. Phys. 16 https://doi.org/10.5194/hacp-16-11601-2016, 11 601–611 615.

Colette, A., Andersson, C., Manders, A., Mar, K., Mircea, M., Pay, M., Raffort, V., Tsyro, S., Cuvelier, C., Adani, M., Bessagnet, B., Bergström, R., Brig- anti, G., Butler, T., Cappelletti, A., Couvidat, F., D'Isidoro, M., Doumbia, T., Fagerli, H., Granier, C., Heyes, C., Klimont, Z., Ojha, N., Otero, N., Schaap, M., Sindelarova, K., Stegehuis, A., Roustan, Y., Vautard, R., van Meijgaard, E., Vivanco, M., Wind, P., 2017. Eurodelta-trends, a multi- model experiment of air quality hindcast in europe over 1990–2010. Geosci. Model Dev. 10, 3255–3276. https://doi.org/10.5194/gmd-10-3255-2017.

de Foy, B., Brune, W.H., Schauer, J.J., 2020. Changes in ozone pho- tochemical regime in fresno, California from 1994 to 2018 deduced from changes in the weekend effect. Environ. Pollut. 263, 114380. https://doi.org/10.1016/j.envpol.2020.114380.

EEA, E.E.A., 2019. Air quality in europe-2019 report. Tech. rep.

EEA, E.E.A., 2020. Air quality in europe-2020 report. Tech. rep.

Emmerson, K., Palmer, P., Thatcher, M., Haverd, V., Guenther, A., 2019. Sensitivity of isoprene emissions to drought over south-eastern Australia: in- tegrating models and satellite observations of soil moisture. Atmospheric BEnvironment 209, 112–124. https://doi.org/10.1016/j.atmosenv.2019.04.038.

European Parliament and Council of the European Union, 2008. Directive 2008/50/ec of the European Parliament and of the Council of 21 May 2008 on Ambient Air Quality and Cleaner Air for Europe. Tech. Rep. European Parlia- ment and Council of the European Union.

Fleming, Z., Doherty, R., Schneidemesser, E., Malley, C., Cooper, O., Pinto, J., Colette, A., Xu, X., Simpson, D., Schultz, M., Lefohn, A., Hamad, S., Moolla, R., Solberg, S., 2018. Tropospheric ozone assessment report : present-day ozone distribution and trends relevant to human healths. Elementa: Science of the Anthropocene 6. https://doi.org/10.1525/elementa.273.

Gerosa, G., Finco, A., Mereu, S., Vitale, M., Manes, F., Denti, A., 2009. Comparison of seasonal variations of ozone exposure and fluxes in a mediter- ranean holm oak forest between the exceptionally dry 2003 and the following year. Environ. Pollut. 157, 1737–1744. https://doi.org/10.1021/acs.est.7b03130.

Guenther, A., Karl, T., Harley, P., Wiedinmyer, C., Palmer, P., Geron, C., 2006. Estimates of global terrestrial isoprene emissions using megan (model of emissions of gases and aerosols from nature). Atmos. Chem. Phys. 6, 3181–3210. https://doi.org/10.5194/acp-6-3181-2006.

Haman, C., Couzo, E., Flynn, J., Vizuete, W., Heffron, B., Lefer, B., 2014. Relationship between boundary layer heights and growth rates with ground- level ozone in houston, Texas. J. Geophys. Res. Atmos. 6230–6245. https://doi.org/10.1002/2013JD020473.

Hastie, T., Tibshirani, R., 1990. Generalized Additive Models. Chapman and Hall, London.

Herbach, H., Dee, D., 2016. Era5 reanalysis is in production. ECMWF Newsl 147, 7.

Horton, D., Skinner, C., Singh, D., Diffenbaugh, N., 2014. Occurrence and persistence of future atmospheric stagnation events. Nat. Clim. Change 698, 4–703. https://doi.org/10.1038/nclimate2272.

Jackson, L., Carslaw, N., Carslaw, D., Emmerson, K., 2009. Modelling trends in oh radical concentrations using generalized additive models. Atmos. Chem. Phys. 9, 2021–2033. https://doi.org/10.5194/acp-9-2021-2009.

Jacob, D., Winner, D., 2009. Effect of climate change on air quality. Atmos. Environ. 43, 51–63.

Jacob, D., Logan, J., Yevich, R., Gardner, G., Spivakovsky, C., Wofsy, S., Munger, J., Sillman, S., Prather, M., Rodgers, M., Westberg, H., Zim- merman, P., 1993. Simulation of summertime ozone over north America. J. Geophys. Res. 98, 14797e14816.

Jing, P., Zifeng, L., Steiner, A., 2017. The ozone-climate penalty in the mid- western u.s. Atmos. Environ. 170 https://doi.org/10.1016/j.atmosenv.2017.09.038, 14797e14816.

Kavassalis, S., Murphy, J., 2017. Understanding ozone-meteorology cor- relations: a role for dry deposition. Geophys. Res. Lett. 44, 2922–2931. https://doi.org/10.1002/2016GL071791.

Kendall, M., 1975. Rank Correlation Methods. Charles Griffin, London.

Kerr, G., Waugh, D., Sarah, S., Steenrod, S., Oman, L., Strahan, S., 2019. Disentangling the drivers of the summertime ozone-temperature relationship over the United States. J. Geophys. Res.: Atmosphere 124, 10503–10524. https://doi.org/10.1029/2019JD030572.

Kulkarni, P., Bortoli, D., Silva, A., 2013. Nocturnal surface ozone enhance- ment and trend over urban and suburban sites in Portugal. Atmos. Environ. 71, 251–259.

LaFranchi, B., Goldstein, A., Cohen, R., 2011. Observations of the temperature dependent response of ozone to nox reductions in the sacra- mento, ca urban plume. Atmos. Chem. Phys. 11, 6945–6960. https://doi.org/10.5194/acp-11-6945-2011.

Leibensperger, E., Mickley, L., Jacob, D., 2008. Sensitivity of us air quality to mid-latitude cyclone frequency and implications of 1980–2006 climate change. Atmos. Chem. Phys. 8, 7075–7086. https://doi.org/10.5194/acp-8-7075-2008.

Lin, M., Horowitz, L., Paulot, F., Malyshev, S., Shevliakova, E., Finco, A., Gerosa, G., Kubistin, D., Pilegaard, K., 2020. Vegetation feedbacks during drought exacerbate ozone air pollution extremes in europe. Nat. Clim. Change 10, 791. https://doi.org/10.1038/s41558-020-0839-4.

Murphy, J., Day, D., Cleary, P., Wooldridge, P., Millet, D., Goldstein, A., Cohen, R., 2007. The weekend effect within and downwind of sacramento part 1: observations of ozone, nitrogen oxides, and voc reactivity. Atmos. Chem. Phys. 7, 5327–5339. https://doi.org/10.5194/acp-7-5327-2007.

Otero, N., Sillmann, J., Rust, H., Butler, T., 2016. Synoptic and mete- orological drivers of extreme ozone concentrations over europe. Environ. Res. Lett. 11, 024005 https://doi.org/10.1088/1748-9326/11/2/024005.

Otero, N., Sillmann, J., Mar, K., Rust, H., Solberg, S., Andersson, C., Engardt, M., Bergström, R., Bessagnet, B., Colette, A., Couvidat, F., Cuvelier, C., Tsyro, S., Fagerli, H., Schaap, M., Manders, A., Mircea, M., Briganti, G., Cappelletti, A., Adani, M., D'Isidoro, M., Pay, M.-T., Theobald, M., Vivanco, M., Wind, P., Ojha, N., Raffort, V., Butler, T., 2018. A multi-model comparison of meteorological drivers of surface ozone over europe. Atmos. Chem. Phys. 18, 12269–12288. https://doi.org/10.5194/acp-18-12269-2018.

Porter, W., Heald, C., 2019. The mechanisms and meteorological drivers of the summertime ozone–temperature relationship. Atmos. Chem. Phys. 19, 13367–13381. https://doi.org/10.5194/acp-19-13367-2019.

Pusede, S., Cohen, R., 2012. On the observed response of ozone to nox and voc reactivity reductions in san joaquin valley California 1995–present. Atmos. Chem. Phys. 12, 8323–8339, 110.5194/acp-12-8323-2012.

Pusede, S., Gentner, D., Wooldridge, P., Browne, E., Rollins, A., Min, K.-E., Russell, A., Thomas, J., Zhang, L., Brune, W., Henry, S., DiGangi, J., Keutsch, F., Harrold, S., Thornton, J., Beaver, M., Clair, J.S., Wennberg, P., Sanders, J., Ren, X., VandenBoer, T.C., Markovic, M.Z., Guha, A., Weber, R., Coldstein, A., Cohen, R., 2014. On the temperature dependence of organic reactivity, nitrogen oxides, ozone production, and the impact of emission controls in san joaquin valley, California. Atmos. Chem. Phys. 14, 3373–3395. https://doi.org/10.5194/acp-14-3373-2014.

Pusede, S., Steiner, A., Cohen, R., 2015. Temperature and recent trends in the chemistry of continental surface ozone. Atmos. Chem. Phys. 115, 3898–3918. https://doi.org/10.1021/cr5006815.

Querol, X., Alastuey, A., Reche, C., Orio, A., Pallares, M., Reina, F., Dieguez, J., Mantilla, E., Escudero, M., Alonso, L., Gangoiti, G., Millán, M., 2016. On the origin of the highest ozone episodes in Spain. Sci. Total Environ. 572, 379–389. https://doi.org/10.1016/j.scitotenv.2016.07.193.

Rasmussen, D., Hu, J., Mahmud, A., Kleeman, M., 2013. The ozone-climate penalty: past, present, and future. Environ. Sci. Technol. 47, 14258–14266, 110.1016/j.atmosenv.2011.11.021.

Romer, P., Duffey, K.C., Wooldridge, P., Edgerton, E., Baumann, K., Feiner, P., Miller, D., Brune, W., Koss, A., de Gouw, J., Misztal, P., Goldstein, A., Cohen, R., 2018. Effects of temperature-dependent nox emissions on continental ozone production. Atmos. Chem. Phys. 18, 2601–2614. https://doi.org/10.5194/acp-18-2601-2018.

Seinfeld, J., Pandis, S., 2006. In: Atmospheric Chemistry and Physics: from Air Pollution to Climate Change, second ed.

Sen, P., 1968. Estimates of the regression coefficient based on kendall's tau. J. Am. Stat. Assoc. 63 (324), 1379–1389. https://doi.org/10.1080/01621459.1968.10480934.

Sicard, P., Coddeville, P., Galloo, J., 2009. Near-surface ozone levels and trends at rural stations in France over the 1995–2003 period. Environ. Monit. Assess. 156, 141–157. https://doi.org/10.1007/s10661-008-0470-8.

Sicard, P., Paoletti, E., Agathokleous, E., Araminien\`e, V., Proietti, C., Coulibaly, F., De Marco, A., 2020. Ozone weekend effect in cities: deep insights for urban air pollution control. Environ. Res. 191, 110193. https://doi.org/10.1016/j.envres.2020.110193.

Sillman, S., 1999. The relation between ozone, nox and hydrocarbons in urban and polluted rural environments. Atmos. Environ. 33, 1821–1845. https://doi.org/10.1016/S1352-2310(98)00345-8.

Sillman, S., Samsom, P., 1995. Impact of temperature on oxidant photo- chemistry in urban, polluted rural and remote environments. J. Geophys. Res. 100, 11497–11508. https://doi.org/10.1029/94JD02146.

Solberg, S., Walker, S., Schneider, P., Guerreiro, C.B.B., Colette, A., 2018. Discounting the Effect of Meteorology on Trends in Surface Ozone: Development of Statistical Tools. ETC/ACM Technical Paper 2017/15.

Steiner, A., Tonse, S., Cohen, R., Goldstein, A., Harley, R., 2006. Influ- ence of future climate and emissions on regional air quality in California. J. Geophys. Res. 111, D18303.

Steiner, A., Davis, A., Sillman, S., Owen, R., Michalak, A., Fiore, A., 2010. Observed suppression of ozone formation at extremely high temperatures due to chemical and biophysical feedbacks. Proc. Natl. Acad. Sci. U.S.A. 107, 19685e19690.

Teuling, A., 2018. Climate hydrology: a hot future for european droughts. Nat. Clim. Change 8, 364–365.

Theil, H., 1950. A rank-invariant method of linear and polynomial regres- sion analysis, 3; confidence regions for the parameters of polynomial regres- sion equations. Stichting Mathematisch Centrum Statistische Afdeling, pp. 1–16. SP 5a/50/R).

Wesely, M., 1989. Parameterization of surface resistances to gaseous dry depo- sition in regional-scale numerical models. Atmos. Environ. 23 (6), 1293–1304. https://doi.org/10.1016/0004-6981(89)90153-4.

Wolff, G., Kahlbaum, D.F., Heuss, J., 2013. The vanishing ozone week- day/weekend effect. J. Roy. Stat. Soc. B 63, 292–299. https://doi.org/10.1080/10962247.2012.749312.

Wood, S., 2006. Low-rank scale-invariant tensor product smooths for general- ized additive mixed models. Biometrics 62 (4), 1025–1036. https://doi.org/10.1111/j.1541-0420.2006.00574.x.

Wood, S., Pya, N., Säfken, B., 2016. Smoothing parameter and model selection for general smooth models. J. Am. Stat. Assoc. 111 (516), 1548–1563. https://doi.org/10.1080/01621459.2016.1180986.

Wu, S., Mickley, L., Leibensperger, E., Jacob, D., Rind, D., Streets, D., 2008. Effects of 2000–2050 global change on ozone air quality in the United States. J. Geophys. Res. Atmospheres 113 (D6), D06302. https://doi.org/10.1029/2007JD008917.

Yan, Y., Lin, J., Pozzer, A., Kong, S., Lelieveld, J., 2019. Rend reversal 960 from high-to-low and from rural-to-urban ozone concentrations over europe. Atmos. Environ. 213, 25–36. https://doi.org/10.1016/j.atmosenv.2019.05.